On the Simulation of Well-Logging Tools for Oil and Gas Exploration Using Unconditionally Stable Time-Domain FDTD Algorithms

***Hwa-Ok Lee*[1], *Fernando L. Teixeira*[1]**

[1]ElectroScience Lab. and Dept. of Electrical and Computer Engineering,
The Ohio State University,
Columbus, OH 43212, U.S.A.,
leehw@ece.osu.edu, teixeira@ece.osu.edu

Abstract

Electromagnetic well logging tools are traditionally used in oil and gas exploration to measure resistivities of the surrounding earth formation. The cylindrical finite-difference time domain (FDTD) method has been popularly applied to solve well logging tool problems because of its matrix-free characteristic and its flexibility to simulate complex geometries. However, the maximum time step in FDTD is limited by the CFL condition, leading to the need of a large number of time steps in highly refined grids. To overcome the CFL condition, an unconditionally stable alternating-direction-implicit (ADI)-FDTD method can be employed. However, ADI-FDTD exhibits increased numerical dispersion errors for large time steps. To reduce the dispersion error, a complex envelope (CE) ADI-FDTD algorithm is introduced here in cylindrical coordinates. The proposed algorithm reduces the computation time while maintaining the dispersion error at acceptable levels.

1. Introduction

The finite-difference time domain (FDTD) algorithm has been widely used to simulate the response of logging-while-drilling (LWD) tools for oil and gas exploration in complex earth formations. The main advantages of FDTD are its simplicity and flexibility to handle complex geometries. However, the maximum time step in FDTD is limited by the Courant-Friedrich-Levy (CFL) condition, which leads to an excessively large number of time steps in highly refined grids. To overcome the CFL condition, an alternating-direction-implicit (ADI) scheme can be adapted for FDTD. However, the time step in ADI-FDTD is still limited by numerical accuracy with increased numerical dispersion error produced for large time steps. To reduce the dispersion error, a complex envelope (CE) ADI-FDTD algorithm is introduced here in cylindrical coordinates. This envelope technique computes slow-varying envelope fields instead of the fast-varying actual fields and leads to reduced dispersion errors for signals close to the carrier frequency [1]. The use of cylindrical coordinates is very important in our application scenario because it allows for the grid to naturally conform to the (cylindrical) geometry of LWD tools and avoids staircasing errors.

The ADI-FDTD can also be augmented with a perfectly matched layer (PML) absorbing boundary conditions to truncate the computation domain. However, neither traditional split-field PML nor unsplit PML implementations are well suited for ADI-FDTD because of larger reflection errors (for a given number of layers) associated with large time steps and/or small spatial grids. In recent years, a convolution PML (CPML) algorithm based on a complex frequency shifted (CFS) stretching and recursive convolution has been proposed [2]. In this paper, these developments are combined to construct a convolution CFS-PML algorithm in three-dimensional (3-D) non-uniform cylindrical grids. The algorithms are validated against both standard FDTD and numerical mode matching (NMM) results.

2. Methodology

The well-known CFL constraint in FDTD can be overcome by employing an ADI technique for the time update. The resulting ADI-FDTD is an unconditionally stable method and then can be used effectively for modeling LWD tool problems in highly refined grids with relaxed time steps. As mentioned above, CPML-ADI-FDTD is a better choice than other traditional PML for LWD scenarios because the former has better performance for absorbing evanescent waves in earth formations with high conductivity (diffusion-type problem).

2.1 Cylindrical CPML

The modified Maxwell's equations in the complex cylindrical coordinates are given as [3]

$$i\omega \mathbf{D} + \sigma \mathbf{E} = \tilde{\nabla} \times \mathbf{H} \quad , \quad i\omega \mathbf{B} = \tilde{\nabla} \times \mathbf{E} \tag{1}$$

where the nabla operator in complex space implements the PML in cylindrical coordinates and can be written as a *modified* nabla operator in terms of real space coordinates as [3]

$$\tilde{\nabla} = \hat{\rho}\frac{1}{s_\rho}\frac{\partial}{\partial\rho} + \hat{\phi}\frac{1}{\tilde{\rho}}\frac{\partial}{\partial\phi} + \hat{z}\frac{1}{s_z}\frac{\partial}{\partial\rho} \tag{2}$$

Here, s_ρ and s_z are the frequency-dependent complex stretching variables referred to the complex frequency (CFS)-PML stretching variables. Eq. (1) is inverse-Fourier-transformed for the time-domain implementation. The resulting convolution factors in the r.h.s. can be efficiently implemented using recursive convolution. Following the ADI technique, the final implicit equations in time domain are split into two sub-steps and the final updated equations involve a tridiagonal system that can be solved in $O(N)$ operations. The azimuth implicit equations caused by the periodic boundary condition along ϕ are solved by the Sherman-Morrison algorithm.

2.2 Cylindrical CE ADI-FDTD Algorithm

In ADI-FDTD, the time step size can be chosen based solely on accuracy considerations (i.e., the CFL criterion is not relevant anymore). The main factors affecting the accuracy of ADI-FDTD are splitting errors and numerical dispersion errors. Both these errors increase for larger time step size Δt. To improve the numerical accuracy of ADI-FDTD, a CE ADI-FDTD can be utilized, whereby the envelope signal (at some central carrier frequency) is used as the field variable. Close to the carrier frequency, CE ADI-FDTD has much reduced splitting and dispersion errors than ADI-FDTD and can dramatically reduce the computation time for narrowband problems by allowing for larger time steps.

In CE ADI-FDTD, the electric and magnetic field components are represented as

$$(H, E) = \Re e\left[\left(\tilde{H}, \tilde{E}\right)e^{j\omega_c t}\right] \tag{3}$$

where $\Re e(\cdot)$ denotes the real part of a complex number and ω_c denotes the carrier frequency. H and E are the original time-domain magnetic and electric fields, while $\tilde{H}$ and $\tilde{E}$ are the associated complex envelope field representations. Substituting Eq. (3) into Maxwell's equation, the so-called CE Maxwell's equations for the envelope electromagnetic fields in lossy media are obtained

$$\varepsilon\frac{\partial\tilde{\mathbf{E}}}{\partial t} + (j\omega_c + \sigma)\tilde{\mathbf{E}} = \nabla\times\tilde{\mathbf{H}}\ , \quad \varepsilon\frac{\partial\tilde{\mathbf{H}}}{\partial t} + (j\omega_c + \sigma)\tilde{\mathbf{H}} = -\nabla\times\tilde{\mathbf{E}} \tag{4}$$

The CE Maxwell's equations (4) are discretized by applying second-order accurate spatial and temporal finite differences, followed by the ADI splitting of each time update step into two substeps.

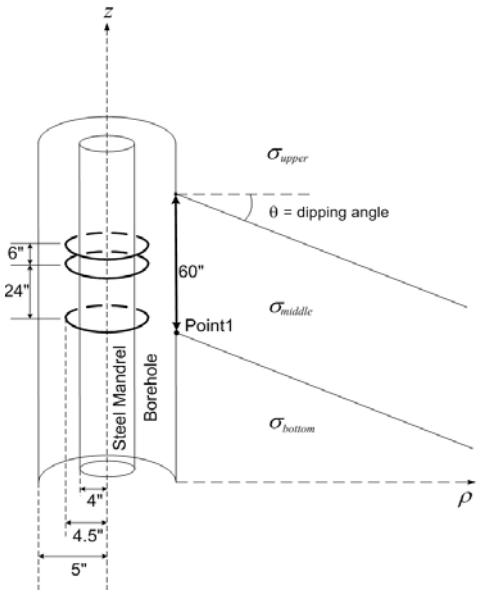

Fig. 1 Illustration of the LWD tool surrounded by a 3-layer formation with dipping beds.

3. Results

The LWD tool considered here has a 4-in radius steel mandrel and is situated inside a 5-in radius borehole, as illustrated in Fig.1. One transmitter and two receivers are employed, consisting of 4.5-in radius loop antennas. The receivers are located 30 and 24 inches away from the transmitter. The excitation is a continuous wave (CW) at 2 MHz. The measurement data of interest are the phase difference (PD) and amplitude ratio (AR) between the two receivers. The steel mandrel surface is modeled as a perfectly electrical conductor (PEC) using a homogeneous Dirichlet boundary condition. Along the radial direction, the region between mandrel and borehole is uniformly discretized, whereas the radial grid cell size outside the borehole is gradually enlarged. The maximum radial grid cell size is chosen by $\Delta\rho_{\max} = \delta_{\min}/6$ at the outer region of the grid, where the smallest skin depth $\delta_{\min}$ is associated with the largest conductivity in the formation. Along the ϕ direction, the grid size $\Delta\phi$ is discretized uniformly via $\Delta l_i = \rho_i \Delta\phi$, $\Delta l_{\max} \le \min(\delta/6\,,\, \lambda/10)$. Along the vertical direction z, the grid size is uniform.

3.1 CPML-ADI-FDTD Results

We first investigate results from the basic CPML-ADI-FDTD algorithm without a complex envelope representation. The computation domain has (N_ρ , N_ϕ , N_z) = (30, 50, 100) nodes and is situated in homogeneous formations. Various resistivities (conductivities) are considered. The radial grid size $\Delta\rho$ is gradually increased form $\Delta\rho_{min}$ = 0.0635cm to $\Delta\rho_{max}$ = 18.765cm, and the uniform grid size along z is 2.54cm. The CPML employs ten cells with cubic taper profiles in both ρ and z directions. The phase difference and amplitude ratio obtained by the CPML-ADI-FDTD algorithm are shown in Fig. 2 for various CFL numbers (CFLN). Recall that the CFLN is given as the ratio of the actual time step by the maximum time step allowed in conventional FDTD. The results match quite well with those of conventional FDTD and NMM, although the time step Δt is six times larger than in the conventional FDTD.

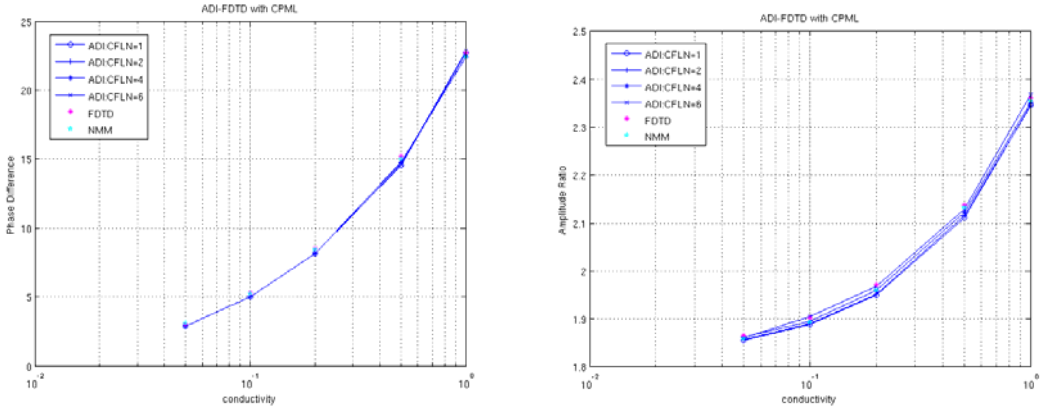

Fig. 2 Phase difference (PD) and Amplitude Ratio (AR) in ADI-FDTD with CPML results against FDTD and NMM results for various CFLN, and different formation conductivities in homogeneous formations.

3.2 CE-ADI-FDTD Results

We next consider the results of the CE-ADI-FDTD algorithm, where a complex envelope representation is used for the fields. The LWD tool again produces a continuous envelope excitation at 2 MHz (carrier frequency f_c). The computation domain is now discretized using (N_ρ , N_ϕ , N_z) = (40, 50, 180) nodes and again different homogeneous formations are considered with various conductivities. The tool geometry is the same as before. The amplitude ratio of ADI-FDTD is shown in Fig. 3, where it is seen that the ADI-FDTD exhibits increasing error against FDTD and NMM as the time step Δt (CFLN) is increased. On the other hand, the CE ADI-FDTD results show reduced errors.

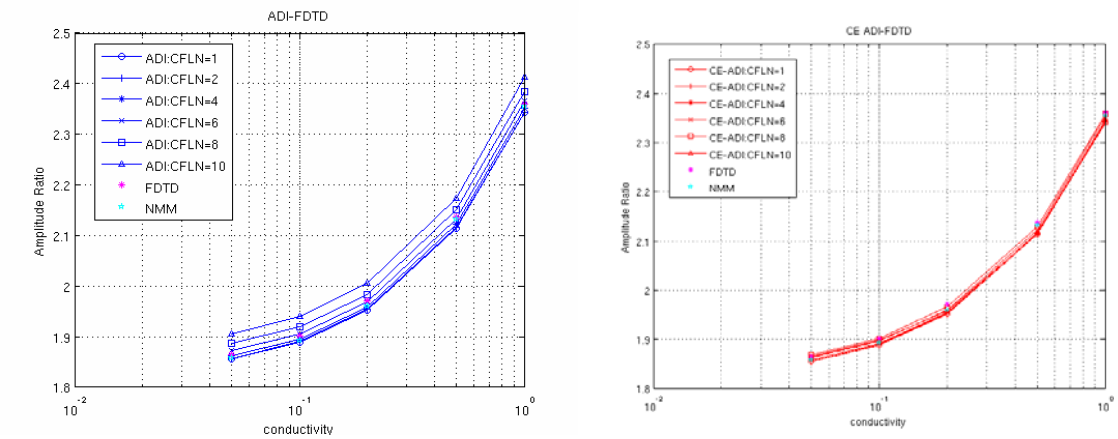

Fig. 3 Amplitude Ratio (AR) in ADI-FDTD and CE ADI-FDTD against FDTD and NMM results for various CFLN, and different formation conductivities in homogeneous formations.

We next validate CE ADI-FDTD results of a LWD tool crossing a 3-layer formation with a dipping bed, as illustrated in Fig. 1, for various dipping angles. The dipping bed thickness is equal to 60 inches along the tool axis as indicated in Fig. 1. Two different dipping angles are considered, viz., $\theta = 0^o$ and $\theta = 45^o$. The computation domain is discretized by $(N_\rho, N_\phi, N_z) = (70, 50, 140)$ nodes. The borehole is filled with a mud of conductivity $\sigma_{mud} = 2$ S/m. Fig. 4 shows that CE ADI-FDTD lead to better results than ADI-FDTD for larger Δt. Note that the NMM algorithm cannot simulate a loop antenna problem with dipping beds at $\theta = 45^o$ and hence is not include in the plot at the right. These results illustrate that CE ADI-FDTD is more accurate in computing the responses of the LWD tools than ADI-FDTD. Furthermore, its unconditional stable property makes it quite suitable to simulate problems in highly refined grids.

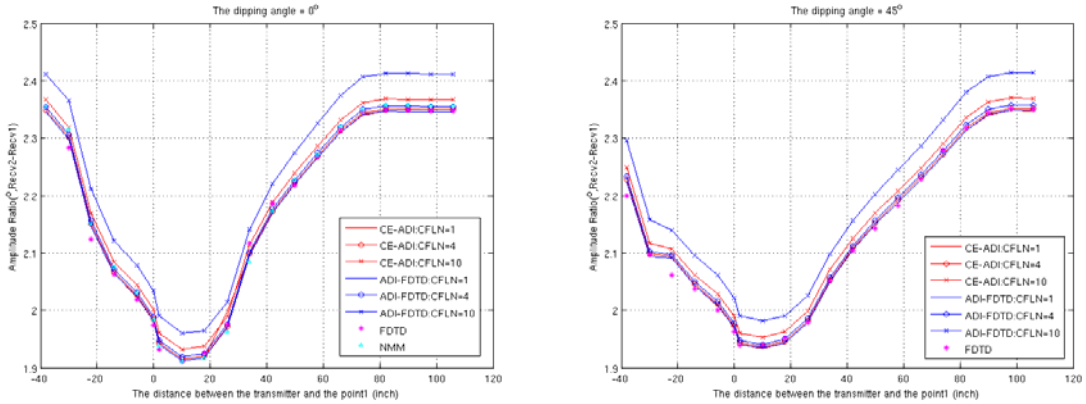

Fig. 4 Amplitude Ratio (AR) in CE ADI-FDTD against ADI-FDT, FDTD and NMM results in 3-layer formation with a dipping bed of 0^o and 45^o for dipping angles.

4. References

1. S. Ju, K.-Y. Jung, and H. Kim, "Investigation on the characteristics of the envelope FDTD based on the alternating direction implicit scheme," *IEEE Microw. Wireless Compon., Lett.*, vol. 13, Sept. 2003, pp. 414-416.

2. S. D. Gedney, G. Liu, J. A. Roden, and A. Zhu, "Perfectly matched layer media with CFS for an unconditionally stable ADI-FDTD method," *IEEE Trans Antennas Propag.*, vol. 49, Nov. 2001, pp. 1554-1559.

3. Y. K. Hue, F. L. Teixeira, L. S. Martin, and M. Bittar, "Three-dimensional simulation of eccentric LWD tool responses in boreholes through dipping formations," *IEEE Trans. Geosci. Remote Sens.*, vol. 2, Feb. 2005, pp. 257-268.